Structure-Dependent Fano Resonances in the Infrared Spectra of Phonons in Few-Layer Graphene

Zhiqiang Li,[1] Chun Hung Lui,[1] Emmanuele Cappelluti,[2,3] Lara Benfatto,[3,4] Kin Fai Mak,[1] G. L. Carr,[5] Jie Shan,[6] and Tony F. Heinz[1,*]

[1]Departments of Physics and Electrical Engineering, Columbia University, 538 West 120th Street, New York, New York 10027, USA
[2]Instituto de Ciencia de Materiales de Madrid, CSIC, 28049 Cantoblanco, Madrid, Spain
[3]Istituto dei Sistemi Complessi, U.O.S. Sapienza, CNR, via dei Taurini 19, 00185 Rome, Italy
[4]Dipartimento di Fisica, Università "La Sapienza", P.le A. Moro 2, 00185 Rome, Italy
[5]Photon Sciences, Brookhaven National Laboratory, Upton, New York 11973, USA
[6]Department of Physics, Case Western Reserve University, 10900 Euclid Avenue, Cleveland, Ohio 44106, USA

(Received 20 September 2011; published 10 April 2012)

The in-plane optical phonons around 200 meV in few-layer graphene are investigated utilizing infrared absorption spectroscopy. The phonon spectra exhibit unusual asymmetric features characteristic of Fano resonances, which depend critically on the layer thickness and stacking order of the sample. The phonon intensities in samples with rhombohedral (*ABC*) stacking are significantly higher than those with Bernal (*AB*) stacking. These observations reflect the strong coupling between phonons and interband electronic transitions in these systems and the distinctive variation in the joint density of electronic states in samples of differing thickness and stacking order.

DOI: 10.1103/PhysRevLett.108.156801 PACS numbers: 73.22.Pr, 63.20.kd, 63.22.Rc, 78.67.Wj

Recent studies have revealed a broad range of novel physical phenomena in few-layer graphene (FLG) [1–8]. The band structure of FLG exhibits a sensitive dependence to both the layer thickness and the stacking sequence of the graphene sheets [1]. It has recently been shown experimentally that, under a perpendicular electric field, samples with Bernal (*AB*) stacking are semimetals [9], whereas those with rhombohedral (*ABC*) stacking are semiconductors with tunable band gaps [6]. Furthermore, new phenomena resulting from many-body interactions and from structurally dependent Berry's phase are expected to occur in FLG [2–5]. Rhombohedrally (*ABC*) stacked FLG, for example, has been predicted to exhibit spontaneous symmetry-breaking ground states, including pseudospin magnetism and various spontaneous quantum Hall states [2], associated with the material's flat bands with diverging density of states (DOS) at low energy and the resulting enhanced electron-electron interactions. In view of these intriguing phenomena, exploring the role of sample thickness and stacking order in the physics of FLG is of great interest.

In this Letter, we report the observation by infrared (IR) spectroscopy of the in-plane optical (*G*-mode) phonons in FLG samples of differing layer number ($N = 3, 4, 5, 6$) and crystallographic stacking sequence. In samples of Bernal (*AB*) stacking and rhombohedral (*ABC*) stacking, the phonon absorption spectra display the distinctive features of Fano resonances [10] arising from the discrete phonon transition embedded in, and interacting with, the continuum of electronic transitions. Both the line shape and intensity of the spectra reveal a dramatic dependence on the sample thickness and stacking order: The phonon feature displays strongly asymmetric line shapes, as well as ones varying from predominantly increased absorption to increased transmission, depending on the physical structure of the FLG sample. Furthermore, the phonon intensities in *ABC*-stacked FLG are substantially (~ 10 times) higher than those in their *AB*-stacked counterparts. We show that in FLG the bare dipole from charge imbalance in the different sublattices of the system is negligible, so all of the observed effects arise from the strong coupling between phonons and electronic excitations in these systems. We provide a theoretical description of our findings in terms of the mixed current-phonon response function recently employed for bilayer graphene [11]. This approach provides a natural means of understanding the relationship between the line shape and intensity of the phonon features, on the one hand, and the electronic structure of the FLG sample, on the other. Our work extends previous studies of the Fano resonance in bilayer graphene [12,13]. In these studies, the material's electronic transitions were tuned with respect to the optical phonons through modification of the band structure and doping level [12,13]. For FLG, such diverse resonant behavior is achieved naturally through the intrinsic electronic properties of FLG of differing physical structure.

We investigated FLG samples deposited on SiO_2/Si substrates by mechanical exfoliation of Kish graphite. IR reflectance and transmission measurements were performed using a Fourier transform IR spectrometer coupled with an IR microscope in the range of photon energy (E) of 0.1–1 eV with a spectral resolution of 0.25 meV. The number of layers for a given sample could be precisely determined from transmission measurements in the

near-IR range (> 0.8 eV), where each graphene monolayer absorbs approximately 2.3% of the light [14–17]. From the reflectance and transmission data, the complex optical conductivity spectra, $\sigma_1(E) + i\sigma_2(E)$, of few-layer graphene were extracted. The analysis takes into account the multiple reflections in the substrate [18].

In samples with three to six layers, two distinct types of absorption spectra $\sigma_1(E)$ were observed for samples with exactly the same number of layers. One class of spectra follows the results previously reported for Bernal stacking [15]. The other class is characterized by two significantly stronger absorption peaks, with positions that shift successively to lower energy with increasing layer numbers (Fig. 1 and Fig. S1 in [19]). Previous studies [8,20] have shown that samples with rhombohedral stacking exhibit such pronounced absorption peaks, which arise because of the high electronic joint density of states (JDOS) near the critical points in the band structure. The evolution of the band structure of rhombohedral samples is also predicted to produce a red shift in the low-energy absorption peaks with increasing layer numbers [21]. The agreement between the second class of spectra and the above expectations indicates the dominance of rhombohedral stacking order in these samples [22].

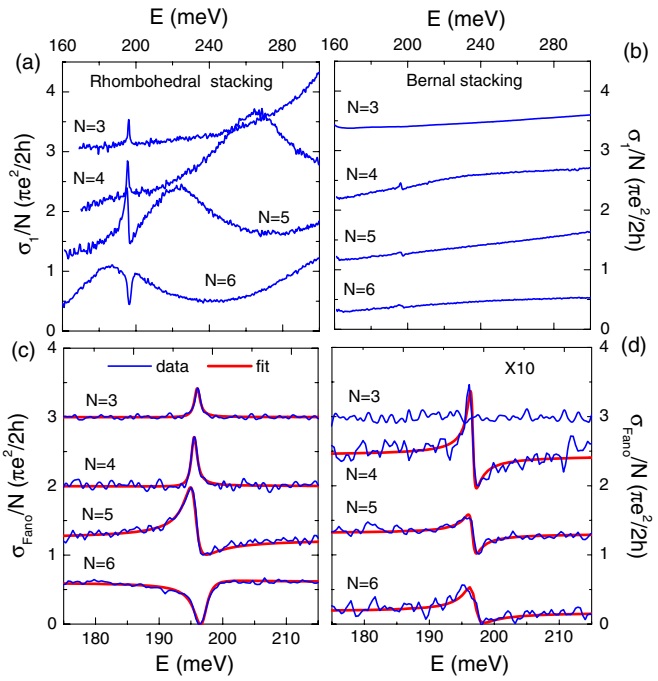

FIG. 1 (color online). (a)–(b) The normalized optical conductivity, $\sigma_1(E)/N$, of N-layer graphene with rhombohedral and Bernal stacking. (c)–(d) The normalized Fano spectra $\sigma_{\mathrm{Fano}}(E)/N$ in the region of the phonon feature for FLG with rhombohedral (c) and Bernal (d) stacking, obtained by subtraction of an electronic background from the data in (a) and (b). The smooth red lines are fits using Eq. (1). The spectra in (d) have been multiplied by a factor of 10. For clarity, the spectra are displaced vertically from one another by increments of $(\pi e^2/2h)$.

In addition to the broad features in the absorption spectra from electronic transitions, we also observed (Fig. 1) pronounced narrow features at ~200 meV, the energy of G-mode (in-plane, Γ-point optical) phonons [23]. These phonons in FLG can be observed in both IR and Raman spectroscopy because the G-mode phonon in graphene splits into N distinct doubly degenerate modes in N-layer graphene, which include both IR-active and Raman-active modes [24]. Moreover, in doped samples, the Raman-active (IR-active) modes can gain some IR (Raman) activity from lowering of the symmetry induced by the doping [12,13,25]. Interestingly, instead of a symmetric resonance feature corresponding to increased absorption normally expected for excitation of these modes, we find both resonance and antiresonance (corresponding to reduced absorption) line shapes, as well as dispersion line shapes. The line shape and intensity of the phonon spectra exhibit striking changes as a function of layer thickness and stacking order. In particular, the phonon features in the rhombohedral samples show much ($\sim 10\times$) higher intensity than those in the Bernal samples.

The data in Fig. 1 were measured for similarly prepared samples with comparable carrier densities, estimated to be around 5×10^{12} cm^{-2}, from unintentional doping [19]. To check the effect of doping on the phonon features, we performed optical measurements on trilayer samples with electrical gating [6]. We found that while the phonon spectra of samples with either stacking order can be continuously tuned by gating, the phonon intensity of *ABC* samples is always much higher than that of *ABA* samples at similar doping levels (except at low doping levels where charge inhomogeneity can complicate the intrinsic physics).

The observed resonance, antiresonance, and dispersion absorption line shapes are characteristic of Fano resonances arising from coupling between the phonons and an electronic continuum [10]. Therefore, in the vicinity of the phonon energy we described the experimental absorption spectra $\sigma_1(E)$ as $\sigma_1(E) = \sigma_e(E) + \sigma_{\mathrm{Fano}}(E)$, where we have separated the smoothly varying background electronic absorption σ_e (E) [19] to highlight the phonon feature. We then compare the result to the Fano resonance line shape [10]:

$$\sigma_{\mathrm{Fano}}(E) = \frac{2p}{\pi\Gamma(q^2+1)}\frac{(q+\varepsilon)^2}{(1+\varepsilon^2)}, \qquad (1)$$

where $\varepsilon = 2(E\text{-}E_{\mathrm{ph}})/\Gamma$, E_{ph}, and Γ are, respectively, the energy and width of the phonon feature. In this expression, p denotes the phonon intensity parameter, which is always positive and vanishes when the phonon feature is absent [11]. The Fano parameter q, which is a real number [26], governs the line shape. When $|q| \gg 1$, we can consider the phonon to dominate the response and a resonance is

observed [Eq. (1) approaches a Lorentzian]; on the other hand, when $|q| \ll 1$, electronic excitation dominates and an antiresonance feature is observed. For intermediate values of $|q| \sim 1$, the electronic and phonon contributions are comparable and a dispersion line shape is present. In our treatment, we consider p and q to be constants over the narrow energy region of the phonon. The experimental data can be well described by Eq. (1) and a broad electronic background. Fitting parameters are shown in Fig. 2, and Fig. S3 in [19].

In N-layer graphene, the weak interlayer coupling leads to the presence of N distinct doubly degenerate modes for the G-mode phonon. However, these splittings are quite small, <1 meV [24], and cannot be resolved spectrally due to the finite width of the phonons. In our fit, we thus treat the observed feature as a single phonon. The parameters from the fit are thus phenomenological quantities representing the combined effect of all IR-active phonons. We note that in contrast to the IR spectra presented here, the Raman spectra of the G-mode phonon in all the few-layer samples do not exhibit significant Fano resonance characteristics. We attribute this difference to the lack of an electronic continuum signal because of the apparent weakness of electronic Raman processes. Such an interacting continuum would be necessary to yield a Fano resonance from the discrete Raman phonon peaks.

We now consider the origin of the strikingly different spectra, and, correspondingly, different phonon strength p and Fano parameter q, for the resonances in FLG of different thickness and stacking order. The observed behavior can be explained qualitatively by the Fano theory, in which parameters p and q can be related to the optical transition

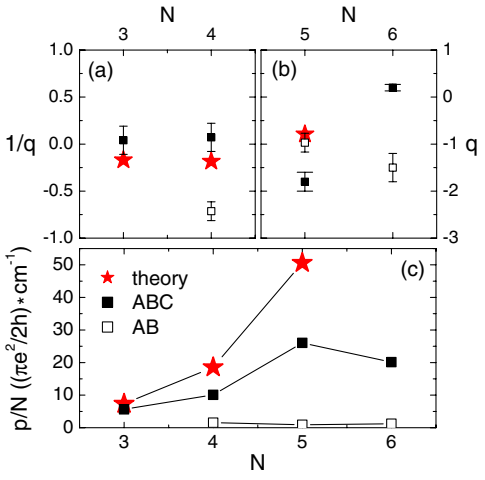

FIG. 2 (color online). (a)–(b) The Fano parameters $1/q$ (q) for Bernal and rhombohedral samples obtained from the fits. The error bars reflect the experimental accuracy and the uncertainty from subtraction of the background. (c) The phonon intensity normalized by layer number, p/N. Theoretical values for rhombohedral samples evaluated using the mixed response function are also shown.

amplitudes of the phonon and electronic continuum, A_{ph} and A_e, and the electron-phonon coupling strength $V_{e\text{-ph}}$: $q = A_{\mathrm{ph}}/\pi V_{e\text{-ph}} A_e$ [10] and $p = |A_{\mathrm{ph}}|^2(1 + 1/q^2)$ [10,11]. In FLG, the optical transition amplitude of a phonon is determined largely by its coupling to the electronic transitions because the bare dipole in these systems is negligible [19]. This coupling, mediated by electron-phonon scattering, reflects the electronic density of states. Thus, to obtain a qualitative understanding of the observed trends, we use the approximation $V_{e\text{-ph}}(E)A_e(E) \sim |A_e(E)|^2$. One can then deduce [19] an expression for the resonant optical transition amplitude of the phonon of

$$A_{\mathrm{ph}}(E_{\mathrm{ph}}) = P \int \frac{dE}{E_{\mathrm{ph}}\text{-}E} |A_e(E)|^2. \tag{2a}$$

Here P denotes the principal value of the integral. Within the same approximation, the Fano line shape parameter q is given by

$$q = \frac{1}{\pi} P \int \frac{dE}{E_{\mathrm{ph}}\text{-}E} \left| \frac{A_e(E)}{A_e(E_{\mathrm{ph}})} \right|^2. \tag{2b}$$

Equations (2a) and (2b) relate the characteristics of the Fano resonance to disposition of the distribution of transition strengths of the electronic continuum $|A_e(E)|^2$ with respect to the phonon energy E_{ph}. Since the weighting of the continuum transitions drops off as the energy moves away from that of the phonon, we expect that the dominant behavior will be determined by the influence of the low-energy interband transition peak (Fig. 1).

This picture offers a natural explanation for the evolution of the Fano parameter q with layer thickness. For rhombohedral FLG samples with three and four layers, the phonon energy lies rather far below the center of the electronic resonance, and $|A_e(E)/A_e(E_{\mathrm{ph}})| \gg 1$ for most parts of the spectrum. Then Eq. (2b) predicts $|q| \gg 1$. For five-layer rhombohedral samples, the phonon lies in the shoulder of the strong electronic transition peak. The large value of $|A_e(E_{\mathrm{ph}})|^2$ leads to a significant reduction of the value of q and, correspondingly, to the observation of a strongly asymmetric phonon feature. Interestingly, the phonon lies near the center of the low-energy electronic resonance in rhombohedral six-layer graphene. In this case, cancellation of the contributions from low ($E < E_{\mathrm{ph}}$) and high ($E > E_{\mathrm{ph}}$) energy sides of the phonon in the integral in Eq. (2b) leads to a rather small value of q (~ 0.2) and a dip feature in the phonon spectrum. Similarly, the phonons in Bernal samples always lie at the low-energy shoulder of the broad electronic resonance peaks (Fig. 1). This yields $|q| \sim 1$ and dispersion-shaped features in the phonon spectra, analogous to the rhombohedral five-layer samples.

The substantial dependence of the phonon intensity $p = |A_{\mathrm{ph}}|^2(1 + 1/q^2)$ on the stacking order and layer thickness

can also be explained qualitatively within this picture. Based on Eqs. (2a) and (2b), the higher phonon intensity in rhombohedral samples arises from their stronger electronic absorption peaks compared to those in Bernal samples. Moreover, the increase of p/N with layer thickness N in rhombohedral samples can be understood as follows: The electronic resonance shifts downwards in energy with increasing N and approaches the phonon energy E_{ph}, leading to larger value of $1/(E_{\mathrm{ph}}\text{-}E)$ in Eqs. (2a) and (2b) and thus greater values of p/N. The slight drop of p/N for rhombohedral six-layer samples stems from the reduction of $A_{\mathrm{ph}}(E_{\mathrm{ph}})$ due to the cancellation effects discussed above. Therefore, the trends for both the phonon line shape (through q) and phonon intensity (through p) can be understood based on the coupling between phonons and low-energy interband transitions.

In order to explain our observations within a more quantitative framework, we note that the functions $A_{\mathrm{ph}}(E)$ and $-\pi V_{e\text{-ph}}(E)A_e(E)$ in FLG are linked by Kramers–Kronig relations in the Fano model due to the negligible bare dipole in these systems [19]; therefore, for each infrared active mode ν, a complex function, the mixed current-electron-phonon response function $\chi_{j\nu}(E)$ [11,19], can be used to describe the phonon amplitude A_{ph} and the electronic continuum amplitude A_e through $\mathrm{Re}\ \chi_{j\nu}(E) = A_{\mathrm{ph}}(E)$ and $\mathrm{Im}\ \chi_{j\nu}(E) = -\pi V_{e\text{-ph}}(E)A_e(E)$. The interference between the real and imaginary parts of $\chi_{j\nu}(E)$ determines the Fano line shape, whereas its absolute value is related to the phonon intensity. In particular, $q_\nu = -\mathrm{Re}\chi_{j\nu}(E_{\mathrm{ph}})/\mathrm{Im}\chi_{j\nu}(E_{\mathrm{ph}})$ and $p_\nu = |\chi_{j\nu}(E_{\mathrm{ph}})|^2$. For systems with multiple bands such as FLG, this response function provides a microscopic description of the contributions of all of the allowed electron-hole excitations to the Fano resonance [11]. Within a standard tight-binding model, we find in the rhombohedral 6-layer samples and in all Bernal samples that several phonon modes are involved in the phonon spectra with comparable intensity [19]. This prevents a direct comparison between our theoretical calculations and the Fano analysis in Fig. 1, which assumes the presence of only one effective mode. On the other hand, the rhombohedral samples with $N \leq 5$ show a single dominant IR-active phonon mode $\bar{\nu}$, which is an antisymmetric mode with the carbon atoms in the ith ($i = 1, 2, \ldots, N$) layer moving exactly out of phase with respect to those of the same sublattice in the $(N + 1 - i)$th layer. Therefore, the Fano parameter q and phonon intensity p in these samples are well-defined within our calculations. As shown in Fig. 2, the evolution of q and p with the number of layers is qualitatively reproduced by our calculations. The disagreement between experimental and theoretical values may reflect the effect of additional interlayer coupling parameters γ_i ($i = 2, 3, 4, 5$), which have been omitted in our model for simplicity.

To explain the substantial difference between rhombohedral and Bernal samples, in Fig. 3 we show the electronic band structure and density of states (DOS) for 5-layer graphene with the two different stacking orderings. In rhombohedral samples, the high DOS points in different bands occur roughly at the same momentum $\mathbf{k}$, leading to singularities in the JDOS and very pronounced peaks in the optical absorption spectra [8]. Moreover, the resonance energy for the lowest interband transition is close to the phonon frequency E_{ph}. These features give rise to substantial spectral weight in the mixed response functions and therefore strong IR phonon intensities in rhombohedral samples (Fig. 3). In particular, the above-mentioned antisymmetric mode in rhombohedral samples ($N < 6$) shows the strongest coupling to the low-energy interband transition; therefore, this mode acquires dominant IR intensity. On the other hand, the absence of singularities in the JDOS in Bernal samples [8] results in a weaker IR intensity of phonons. An additional factor contributing to the relative weakness of the phonon feature in Bernal FLG is the presence of several IR-active phonons in these

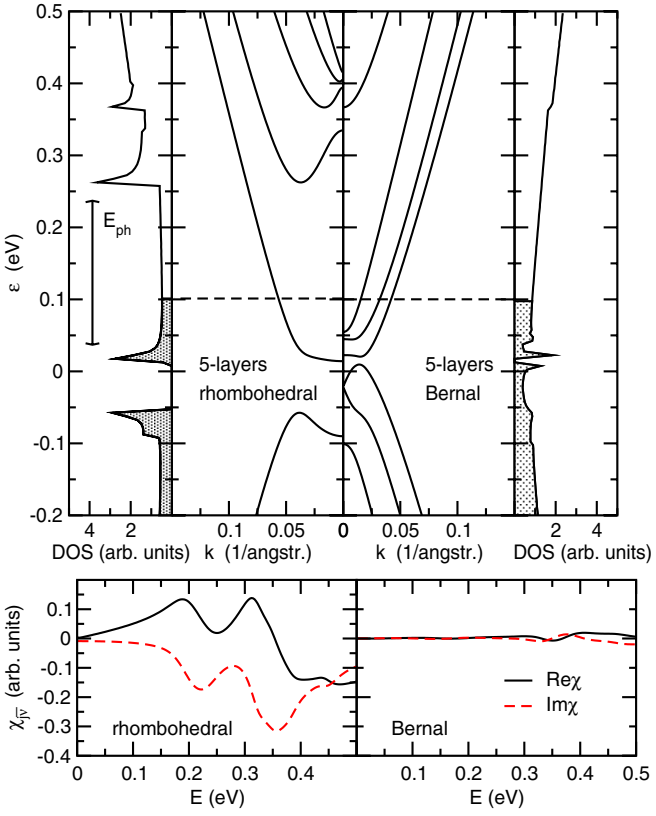

FIG. 3 (color online). Upper panels: A representation of the electronic band structure and DOS for 5-layer graphene samples with rhombohedral and Bernal stacking. The dashed line represents the chemical potential, shifted from charge neutrality because of unintentional doping. Lower panels: The real and imaginary part of the corresponding mixed current-phonon response function responsible for the IR activity.

materials [19]. Since the different phonons have somewhat different frequencies and may have different values of the corresponding Fano parameter q, the observed spectrum arising from the sum of several such asymmetric lines is expected to exhibit cancellation effects.

In summary, we have observed features associated with the zone-center optical phonons in FLG of both Bernal and rhombohedral stacking. The phonon features exhibit Fano resonance line shapes that arise from coupling to the electronic continuum. Our study has revealed 2 important degrees of freedom in defining the characteristics of the Fano response: The layer thickness and crystallographic stacking sequence. This leads to a wide diversity in the observed line shape for different FLG samples without any external modification of properties. The significantly enhanced phonon intensity in rhombohedrally stacked FLG compared to that in the conventional Bernal stacked FLG reflects the distinctive electronic structure of these materials and the corresponding presence of strong, sharply defined low-energy electronic transitions.

This work was supported by the National Science Foundation under Grant No. DMR-0907477 at Case Western Reserve and under Grants No. DMR-1106225 and No. CHE-0641523 at Columbia, with additional funding from NYSTAR. E. C. acknowledges support from the European FP7 Marie Curie Project No. PIEF-GA-2009-251904. The IR measurements were performed at the National Synchrotron Light Source, which is funded by the U.S. DOE under Contract No. DE-AC02-98CH10886.

*Corresponding author: tony.heinz@columbia.edu

[1] F. Guinea, A. H. Castro Neto, and N. M. R. Peres, Phys. Rev. B **73**, 245426 (2006); M. Aoki and H. Amawashi, Solid State Commun. **142**, 123 (2007); S. Latil and L. Henrard, Phys. Rev. Lett. **97**, 036803 (2006); A. A. Avetisyan, B. Partoens, and F. M. Peeters, Phys. Rev. B **80**, 195401 (2009); M. Koshino, Phys. Rev. B **81**, 125304 (2010); S. B. Kumar and J. Guo, Appl. Phys. Lett. **98**, 222101 (2011); B. R. Wu, Appl. Phys. Lett. **98**, 263107 (2011); K. Tang, R. Qin, J. Zhou, H. Qu, J. Zheng, R. Fei, H. Li, Q. Zheng, Z. Gao, and J. Lu, J. Phys. Chem. C **115**, 9458 (2011).

[2] H. Min and A. H. MacDonald, Prog. Theor. Phys. Suppl. **176**, 227 (2008); H. Min and A. H. MacDonald, Phys. Rev. B **77**, 155416 (2008); F. Zhang, J. Jung, G. A. Fiete, Q. Niu, and A. H. MacDonald, Phys. Rev. Lett. **106**, 156801 (2011); F. Zhang, B. Sahu, H. Min, and A. H. MacDonald, Phys. Rev. B **82**, 035409 (2010).

[3] E. McCann and V. I. Fal'ko, Phys. Rev. Lett. **96**, 086805 (2006); J. L. Manes, F. Guinea, and M. A. H. Vozmediano, Phys. Rev. B **75**, 155424 (2007); M. Koshino and E. McCann, Phys. Rev. B **80**, 165409 (2009).

[4] M. Otani, M. Koshino, Y. Takagi, and S. Okada, Phys. Rev. B **81**, 161403 (2010).

[5] J.-A. Yan, W. Y. Ruan, and M. Y. Chou, Phys. Rev. B **79**, 115443 (2009).

[6] C. H. Lui, Z. Q. Li, K. F. Mak, E. Cappelluti, and T. F. Heinz, Nature Phys. **7**, 944 (2011).

[7] L. Zhang, Y. Zhang, J. Camacho, M. Khodas and I. Zaliznyak, Nature Phys. **7**, 953 (2011); W. Bao *et al.*, Nature Phys. **7**, 948 (2011); A. Kumar, W. Escoffier, J. M. Poumirol, C. Faugeras, D. P. Arovas, M. M. Fogler, F. Guinea, S. Roche, M. Goiran, and B. Raquet, Phys. Rev. Lett. **107**, 126806 (2011); S. H. Jhang *et al.*, Phys. Rev. B **84**, 161408(R) (2011).

[8] K. F. Mak, J. Shan, and T. F. Heinz, Phys. Rev. Lett. **104**, 176404 (2010).

[9] M. F. Craciun, S. Russo, M. Yamamoto, J. B. Oostinga, A. F. Morpurgo and S. Tarucha, Nature Nanotech. **4**, 383 (2009).

[10] U. Fano, Phys. Rev. **124**, 1866 (1961).

[11] E. Cappelluti, L. Benfatto, and A. B. Kuzmenko, Phys. Rev. B **82**, 041402 (2010).

[12] A. B. Kuzmenko, L. Benfatto, E. Cappelluti, I. Crassee, D. van der Marel, P. Blake, K. S. Novoselov, and A. K. Geim, Phys. Rev. Lett. **103**, 116804 (2009).

[13] T.-T. Tang *et al.*, Nature Nanotech. **5**, 32 (2009).

[14] K. F. Mak, M Y. Sfeir, Y. Wu, C. H. Lui, J. A. Misewich, and T. F. Heinz, Phys. Rev. Lett. **101**, 196405 (2008).

[15] K. F. Mak, M. Y. Sfeir, J. A. Misewich, and T. F. Heinz, Proc. Natl. Acad. Sci. U.S.A. **107**, 14999 (2010).

[16] R. R. Nair, P. Blake, A. N. Grigorenko, K. S. Novoselov, T. J. Booth, T. Stauber, N. M. R. Peres and A. K. Geim, Science **320**, 1308 (2008).

[17] P. E. Gaskell, H. S. Skulason, C. Rodenchuk, and T. Szkopek, Appl. Phys. Lett. **94**, 143101 (2009).

[18] Z. Q. Li, E. A. Henriksen, Z. Jiang, Z. Hao, M. C. Martin, P. Kim, H. L. Stormer, and D. N. Basov, Nature Phys. **4**, 532 (2008).

[19] See Supplemental Material at http://link.aps.org/supplemental/10.1103/PhysRevLett.108.156801 for more details.

[20] H. Min and A. H. MacDonald, Phys. Rev. Lett. **103**, 067402 (2009).

[21] J.-A. Yan, W. Y. Ruan, and M. Y. Chou, Phys. Rev. B **83**, 245418 (2011).

[22] Note that although Bernal and rhombohedral stacking are the two most stable configurations in three and four layer samples [M. Aoki and H. Amawashi, Solid State Commun. **142**, 123 (2007)], other stacking sequences might be possible in samples with five and six layers. Nevertheless, the data in Fig. 1 indicate that rhombohedral segments are dominant in the second class of samples.

[23] R. Saito, M. Hofmannb, G. Dresselhausc, A. Joriod and M. S. Dresselhaus, Adv. Phys. **60**, 413 (2011).

[24] J.-A. Yan, W. Y. Ruan, and M. Y. Chou, Phys. Rev. B **77**, 125401 (2008).

[25] T. Ando, J. Phys. Soc. Jpn. **76**, 104711 (2007); L. M. Malard, D. C. Elias, E. S. Alves, and M. A. Pimenta, Phys. Rev. Lett. **101**, 257401 (2008).

[26] A. A. Clerk, X. Waintal, and P. W. Brouwer, Phys. Rev. Lett. **86**, 4636 (2001).